Molecular Therapy
Nucleic Acids
Original Article

Inhalation of an RNA aptamer that selectively binds extracellular histones protects from acute lung injury

Beilei Lei,[1] Chaojian Wang,[1] Kamie Snow,[1] Murilo E. Graton,[1,2] Robert M. Tighe,[1] Ammon M. Fager,[1,4] Maureane R. Hoffman,[3,4] Paloma H. Giangrande,[5] and Francis J. Miller, Jr.[1,6,7]

[1]Department of Medicine, Duke University, Durham, NC 27710, USA; [2]São Paulo State University, School of Dentistry, Campus of Aracatuba, São Paulo 16015-050, Brazil; [3]Department of Pathology, Duke University, Durham, NC 27710, USA; [4]Veterans Affairs Medical Center, Durham, NC 27705, USA; [5]Wave Life Sciences, Cambridge, MA 02138, USA; [6]Veterans Affairs Tennessee Valley Healthcare, Nashville, TN 37212, USA; [7]Department of Medicine, Vanderbilt University Medical Center, Nashville, TN 37240, USA

Acute lung injury (ALI) is a syndrome of acute inflammation, barrier disruption, and hypoxemic respiratory failure associated with high morbidity and mortality. Diverse conditions lead to ALI, including inhalation of toxic substances, aspiration of gastric contents, infection, and trauma. A shared mechanism of acute lung injury is cellular toxicity from damage-associated molecular patterns (DAMPs), including extracellular histones. We recently described the selection and efficacy of a histone-binding RNA aptamer (HBA7). The current study aimed to identify the effects of extracellular histones in the lung and determine if HBA7 protected mice from ALI. Histone proteins decreased metabolic activity, induced apoptosis, promoted proinflammatory cytokine production, and caused endothelial dysfunction and platelet activation *in vitro*. HBA7 prevented these effects. The oropharyngeal aspiration of histone proteins increased neutrophil and albumin levels in bronchoalveolar lavage fluid (BALF) and precipitated neutrophil infiltration, interstitial edema, and barrier disruption in alveoli in mice. Similarly, inhaling wood smoke particulate matter, as a clinically relevant model, increased lung inflammation and alveolar permeability. Treatment by HBA7 alleviated lung injury in both models of ALI. These findings demonstrate the pulmonary delivery of HBA7 as a nucleic acid-based therapeutic for ALI.

INTRODUCTION

Acute lung injury (ALI) results from various causes, including inhalation of toxic substances, aspiration of gastric contents, bacterial infection, epidemic viruses, radiation, severe burns, and trauma. Patients with severe ALI often develop acute respiratory distress syndrome (ARDS). The exudative phase of ARDS consists of the activation of resident alveolar macrophages, infiltration of neutrophils, release of proinflammatory cytokines, and injury to epithelial and endothelial cells, resulting in loss of barrier integrity, interstitial and intra-alveolar edema, and impaired gas exchange.[1,2] The ALI incidence in the US is approximately 200,000 people annually, with a mortality rate of ∼40%.[3] However, the treatment of ALI focuses primarily on supportive measures, as there are no effective pharmacotherapies that meaningfully interrupt the progression of injury.

Circulating histone levels are positively associated with the severity and mortality of ARDS.[4–7] Extracellular histones are also detected in bronchoalveolar fluid (BALF) from patients with ALI.[7–10] There are five subtypes of histone proteins, including the linker histone H1 and four core histones, H2A, H2B, H3, and H4. Histones are positively charged and normally associate with DNA in the nucleosome.[11] However, in response to tissue injury or stress, histones are released into the extracellular space from injured cells, during the formation of neutrophil extracellular traps (NETs), or within exosomes from activated macrophages.[12–14] Extracellular histones cause tissue toxicity by increasing intracellular calcium levels and altering membrane permeability.[4,15,16] In addition, they act as damage-associated molecular patterns (DAMPs), activate Toll-like receptors (TLRs), promote proinflammatory cytokine release,[17–20] induce platelet activation and aggregation, and cause microvascular thrombosis.[16,21–25] Their ability to amplify tissue damage provides a strong rationale for targeting extracellular histones in conditions predisposing to ALI.

We identified several histone-binding RNA aptamers using systemic evolution of ligands by exponential enrichment technology with high affinity and specificity to histone proteins H3 and H4.[16,26] RNA aptamers are synthetic single-stranded oligonucleotides that bind to their targets based on their sequence and structure.[27–29] We reported that RNA aptamer KU7 has binding constants with histones at nanomolar levels and does not appreciably bind to other serum proteins.[16] In the current study, we hypothesized that extracellular histones are an essential mediator of lung injury, and the histone-binding aptamer

Received 9 August 2022; accepted 15 February 2023;
https://doi.org/10.1016/j.omtn.2023.02.021.

Correspondence: Francis J. Miller, MD, Department of Medicine, Vanderbilt University Medical Center, Nashville, TN 37240, USA.
E-mail: francis.miller@vumc.org

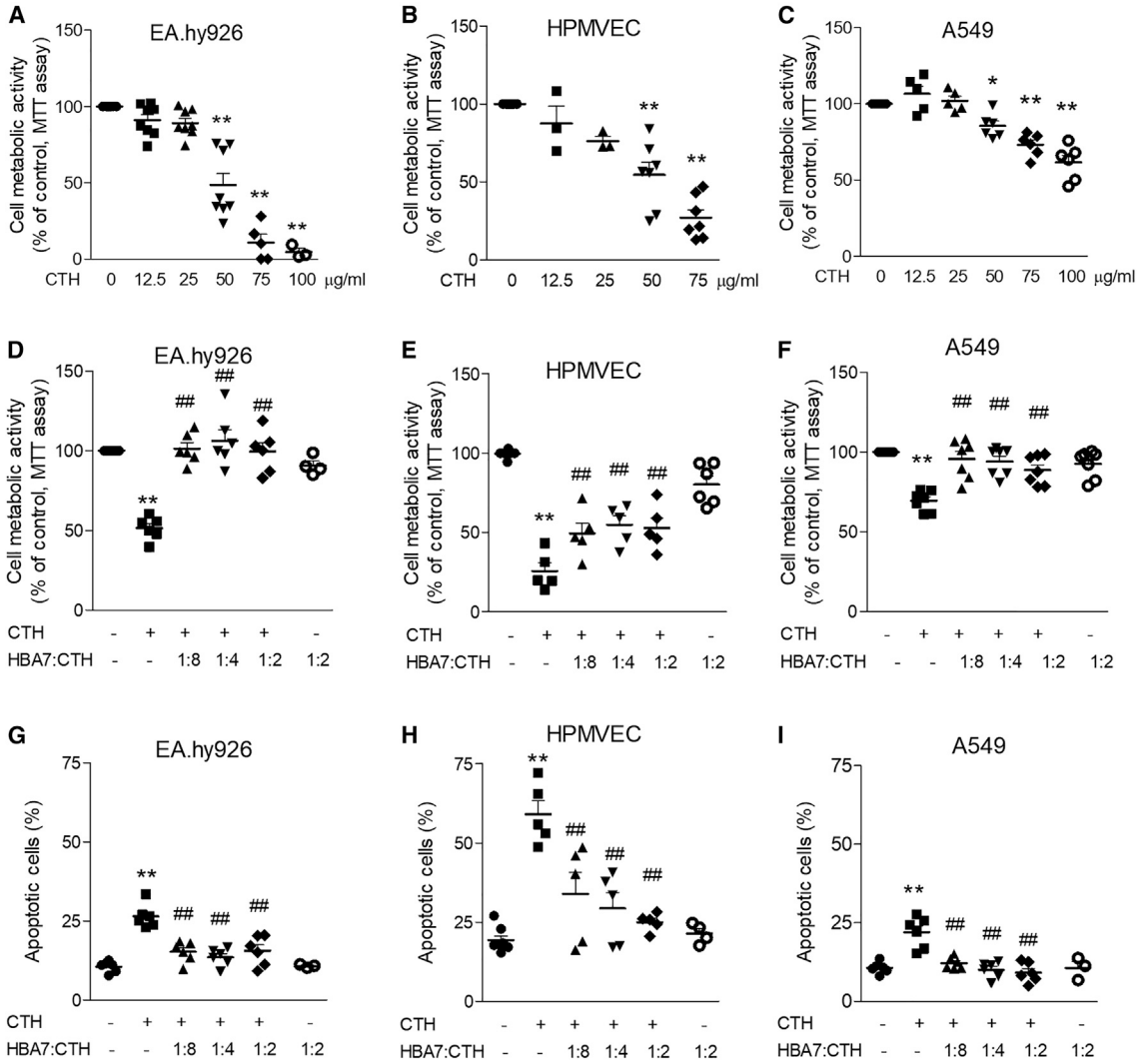

Figure 1. RNA aptamer HBA7 prevents histone-induced cytotoxicity

The dose responses of calf thymus histones (CTHs) in cellular metabolic activity (A–C). The effect of aptamer HBA7 on histone-mediated toxicity (D–F) and cell apoptosis (G–I, total apoptotic cell counts measured by Annexin V staining). Human endothelial EA.hy926 cells were incubated with 50 μg/mL CTH for 24 h. Human pulmonary microvascular endothelial cells (HPMVECs) and human epithelial A549 cells were treated with 75 μg/mL CTH for 4 and 24 h, respectively. HBA7 was added to cells 30 or 60 min after CTH. The ratio refers to the molar ratio of HBA7 to CTH. Data are mean ± SEM, n = 3–8 independent experiments. $^{**}p < 0.01$ vs. control; $^{\#\#}p < 0.01$ vs. CTH.

HBA7 (previously referred to as KU7) would protect mice from ALI in response to wood smoke particulate matter.

A portion of the results was previously reported as an abstract.[30]

RESULTS

RNA aptamer HBA7 prevents histone-mediated cytotoxicity in cultured cells

Human pulmonary endothelial cells (EA.hy926), human pulmonary microvascular endothelial cells (HPMVECs), and human pulmonary epithelial cells (A549) were exposed to calf thymus histones (CTHs). CTHs were used because they represent a biologically relevant mixture of post-translationally modified histone proteins compared with a recombinant histone protein. CTHs caused a concentration-dependent decrease in cellular metabolic activity as measured by MTT assay in all three cell types (Figures 1A–1C). CTH concentrations greater than 50 μg/mL significantly decreased cellular metabolic activity and were chosen for subsequent experiments to evaluate the protective efficacy of HBA7. Administration of CTH reduced cellular metabolic activity (Figures 1D–1F) and induced cell apoptosis (Figures 1G–1I) in EA.hy926 cells, HPMVECs, and A549 cells. Concentration of HBA7 to CTH at molar ratios of 1:8, 1:4, and 1:2 were delivered 30 min after CTH, which rescued cellular metabolic activity and prevented apoptosis. Importantly, HBA7 alone did not affect cellular metabolic activity or apoptosis. The representative cytometry plots of the apoptosis data are provided as a Figure S1.

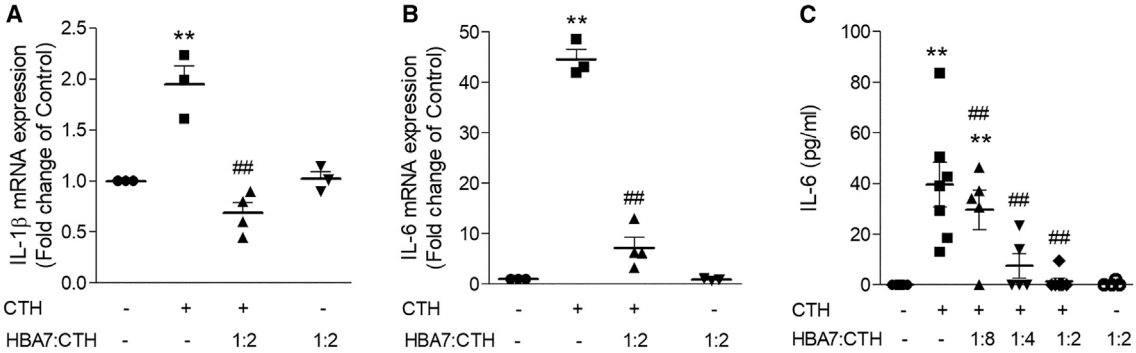

Figure 2. HBA7 prevents histone-mediated upregulation of proinflammatory cytokines

The mRNA expression of cytokines IL-1β (A) and IL-6 (B) in human pulmonary microvascular endothelial cells was measured at 4 h after CTHs (75 μg/mL) challenge. Protein levels of IL-6 in cell supernatants (C) was measured by ELISA. HBA7 was added 30 min after CTH exposure. The ratio refers to the molar ratio of HBA7 to CTH. Data are mean ± SEM, n = 3–8. $^{**}p < 0.01$ vs. control; $^{\#\#}p < 0.01$ vs. CTH.

HBA7 inhibits histone-mediated upregulation of proinflammatory cytokines

Exposure of HPMVECs to CTHs (75 μg/mL) for 4 h increased mRNA expression of the proinflammatory cytokines interleukin-1β (IL-1β) and IL-6 (Figures 2A and 2B). CTH also increased IL-6 protein levels in the cell supernatants measured by ELISA (Figure 2C), whereas IL-1β protein levels did not significantly change from control levels (below detectable limits). The addition of aptamer HBA7 30 min after exposure to CTH prevented the generation of cytokines, while HBA7 alone did not stimulate cytokine production (Figure 2).

HBA7 prevents histone-mediated endothelial dysfunction and platelet activation

Endothelial dysfunction and platelet activation cause pulmonary microvascular thrombosis and contribute to lung injury.[31,32] Intercellular adhesion molecule (ICAM) attracts neutrophils to adhere to endothelial cells,[33] whereas von Willebrand factor (vWF) facilitates platelet adhesion and activation in hemostasis and thrombosis.[34,35] Both ICAM and vWF are markers of endothelial dysfunction. The incubation of EA.hy926 cells (Figures 3A and 3B) and HPMVECs (Figures 3C and 3D) with CTH for 4–6 h promoted the release of ICAM and vWF into the culture media. Treatment with HBA7 after CTH resulted in a concentration-dependent reduction in ICAM and vWF (Figure 3).

P-selectin is expressed on the surface of activated platelets and is involved in platelet aggregation.[36–38] Exposure of human platelets to CTH for 15 min induced P-selectin surface expression (Figure 3E). HBA7 administered with histones prevented platelet activation, while HBA7 alone did not affect platelet activation. In contrast, HBA7 did not inhibit thrombin-mediated platelet activation.

Lung distribution and retention of inhaled Alexa 647-HBA7 in mice

Potential advantages of delivering HBA7 via inhalation include targeted delivery to the lung and greater retention of the aptamer at the site of injury. Before testing the *in vivo* efficacy of HBA7 in preventing lung injury in mice, we first assessed the distribution and retention of HBA7 in the lung and other organs after pulmonary delivery. A fluorescent-tagged Alexa 647-HBA7 was delivered to mice via oropharyngeal aspiration. Tissues and BALF were collected at 4 and 24 h after aptamer administration. Histologic sectioning through the lungs demonstrated Alexa 647 in all lobes and at both time points (Figure 4), while no fluorescent signal was detected in phosphate-buffered saline (PBS)-treated control lungs. These findings are consistent with the distribution of microspheres after oropharyngeal aspiration.[39] The Alexa 647 signal was not observed in the heart, liver, kidney, spleen, or brain. The amount of HBA7 retained in the lungs at 24 h was less than 15% of that recovered at 4 h as measured by fluorescence intensity in BALF (339.2 ± 129.9 vs. 46 ± 5.6 nM, n = 3) and by RT-PCR using RNA extracted from lung tissues (12 ± 2.5 vs. 0.8 ± 0.1 pmol/10 mg tissue; n = 3).

Inhalation of HBA7 protects from histone-mediated ALI in mice

We first evaluated the *in vivo* efficacy of HBA7 in a proof-of-concept histone-mediated lung injury model. CTH was administered to mice via oropharyngeal aspiration. HBA7 was delivered at the same time as histones or 30 min before or 30 min after histones. BALF and organs were collected 8 h after the histone challenge (Figure 5).

The number of macrophages (Figure 5A) and neutrophils (Figure 5B) in BALF increased within 8 h after exposure to CTH. The administration of HBA7 concurrently with histones completely prevented histone-mediated white blood cell (WBC) infiltration. However, the administration of HBA7 30 min before or after the histones did not reduce histone-induced WBC counts in BALF.

The cytokine IL-6 is produced by various cell types in response to TLR activation. IL-6 levels in the BALF increased after exposure to CTH (Figure 5C). HBA7 blocked the production of IL-6 when administered with histones but not with pre- or post-treatment. These findings suggest that the cellular signals responsible for initiating the infiltration of WBCs and producing IL-6 occur immediately or at very low concentrations of histones.

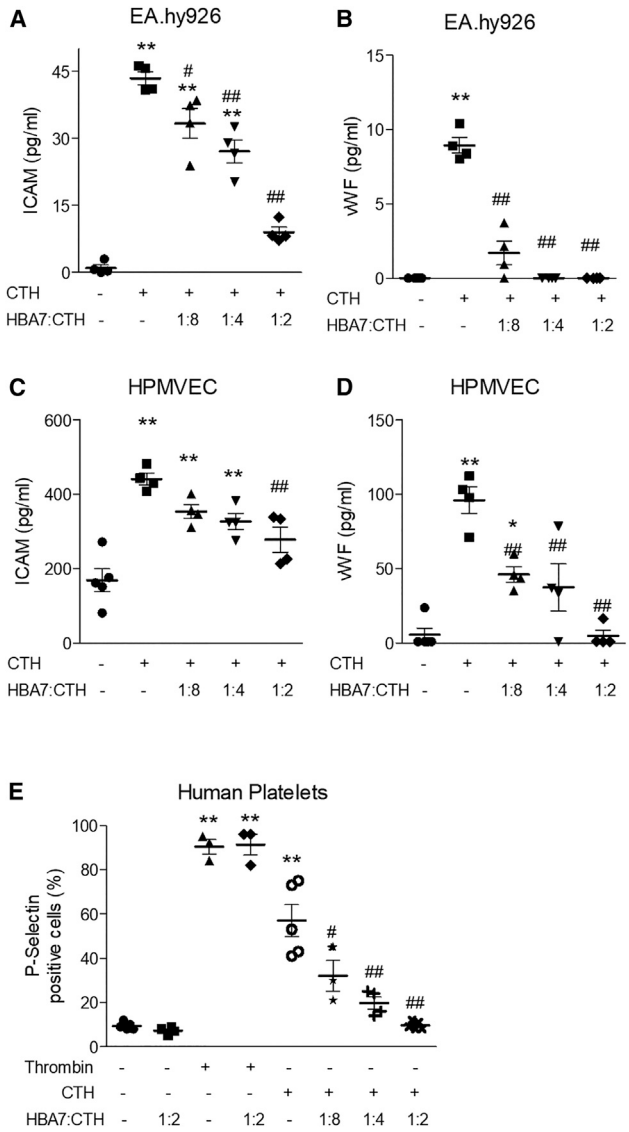

Figure 3. HBA7 prevents histone-mediated endothelial cell dysfunction and platelet activation

Human endothelial EA.hy926 cells (A and B) were incubated with 50 μg/mL CTH for 6 h. HPMVECs (C and D) were treated with 75 μg/mL CTH for 4 h. Intercellular adhesion molecule (ICAM) and von Willebrand factor (vWF) were measured in cell supernatants by ELISA. Aptamer HBA7 was added 30–60 min after CTH. n = 4–7. (E) HBA7 prevents histone-mediated platelet activation. Human platelets were exposed to CTH (50 μg/mL) for 15 min, and platelet activation marker P-selectin expression was measured by flow cytometry. Aptamer HBA7 was added at the same time as the CTH. The ratio refers to the molar ratio of HBA7 to CTH. n = 3–5. *$p < 0.05$, **$p < 0.01$ vs. control; #$p < 0.05$, ##$p < 0.01$ vs. CTH. Data are mean ± SEM.

Increased pulmonary vascular permeability is a hallmark of ALI and ARDS. Therefore, we measured albumin levels in BALF to assess for alveolar-capillary membrane damage. Inhalation of CTH increased albumin in the BALF (Figure 5D). In contrast to the effects of HBA7 on WBCs, HBA7 attenuated the movement of albumin into the alveoli at each time tested (Figure 5D). These data indicate that HBA7 protects from barrier disruption despite the presence of WBCs in the BALF.

Histological examination showed neutrophil infiltration, alveolar destruction, and interstitial edema in histone-treated lungs compared with saline-treated control lungs (Figure 5E). HBA7 alleviated the alveolar damage caused by histones (Figure 5). The delivery of HBA7 alone did not increase WBC, IL-6, or albumin levels in BALF (Figures 5A–5D) and caused no histopathologic changes (Figure 5E).

Efficacy of HBA7 in a wood smoke inhalation model of ALI

Smoke inhalation injury is the leading cause of death due to fires. A primary cause of pulmonary damage is the inhalation of particulate matter. Smoke particulate matter deposits along the mucosa and alveoli to initiate local tissue and alveolar injury.[40] We tested the efficacy of HBA7 in a clinically relevant model of ALI by delivering eucalyptus flaming smoke particulate matter (PM) to mice via oropharyngeal aspiration.[41]

Inflammation and alveolar permeability were increased 24 h after PM, as evident by total WBC, macrophage, and neutrophil counts (Figures 6A–6C), the release of proinflammatory cytokines (Figures 6D and 6E), and albumin (Figure 6F) in BALF. HBA7 delivered by oropharyngeal aspiration 30 min before (HBA7+PM), at the same time as (PM/HBA7), or 30 min after (PM+HBA7) smoke particulate exposure decreased WBC and neutrophil counts, inhibited cytokine release, and reduced alveolar albumin in BALF. Histone H3 levels were increased in the BALF of PM-challenged mice (Figures 6G and 6H), and administration of HBA7 decreased H3 levels. Histological examination of the lungs showed that PM exposure caused neutrophil infiltration to alveoli and interstitial edema (Figures 6I and 6J). Administration of HBA7 reduced lung injury to PM each time point administered (Figures 6I and 6J).

DISCUSSION

There are multiple causes of ALI, including inhaling toxic substances, infection, aspiration of gastric contents, radiation, and trauma. Patients with severe ALI will progress to ARDS, with a high risk of morbidity and mortality. Tissue damage in the lung releases DAMPs, including histone proteins. Histones normally reside in the nucleus, where they partner with DNA. However, when released from damaged cells, histones propagate tissue injury via activation of TLRs, calcium influx, platelet aggregation, and cell death. Because histones (cationic proteins) normally associate with DNA in the nucleosome, we hypothesized that RNA aptamers (anionic molecules) would have extraordinarily high affinity and specificity for histones, making them an ideal reagent for neutralizing extracellular histones. In this study, we tested the efficacy of histone-binding RNA aptamer HBA7 in preventing ALI. *In vitro* studies revealed that extracellular histones were toxic to lung endothelial and epithelial cells and promoted proinflammatory cytokine production and caused endothelial dysfunction and platelet activation. Furthermore, the aspiration of

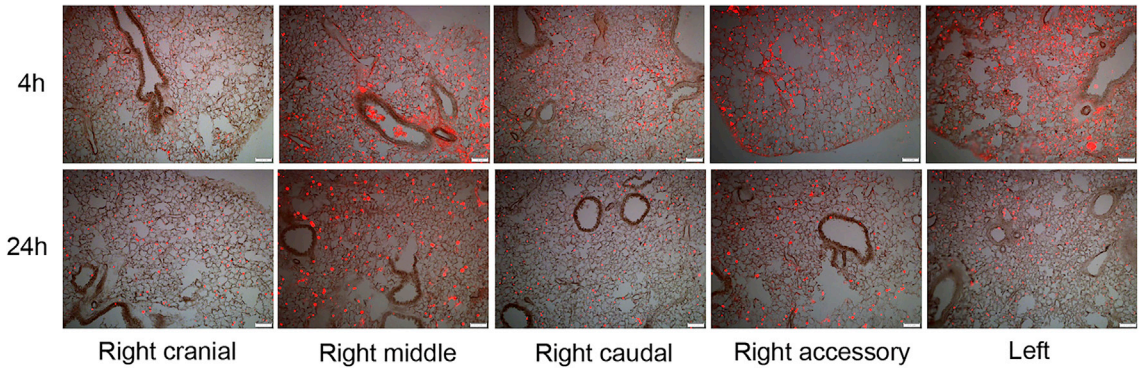

Figure 4. Lung distribution and retention of inhaled Alexa 647-HBA7 in mice

Microscopy images showed lung distribution of Alexa 647-HBA7 at 4 and 24 h after delivery. The fluorescent-tagged aptamer Alexa 647-HBA7 (1.7 nmol, 30 μg) was delivered to C57BL/6 mice via oropharyngeal aspiration. Scale bar is 100 μm.

histones by mice caused alveolar infiltration of macrophages and neutrophils and barrier disruption. The delivery of HBA7 attenuated histone-mediated injury *in vitro* and *in vivo*. Finally, in a clinically relevant model, the pulmonary delivery of HBA7 before, during, or after exposure to smoke PM alleviated ALI.

Cells demonstrate a threshold response to histones such that as the concentration of histones increases, their toxicity also increases. Thus, a strategy of neutralizing histones to maintain a concentration below irreversible tissue damage has the potential to be clinically valuable. We found evidence to support this concept both *in vitro* and *in vivo*. For example, HBA7 prevented cell death at molar concentrations of 1:8 HBA7:CTH. This observation suggests that a molecule of aptamer can neutralize several molecules of histone proteins. However, higher aptamer concentrations were necessary to prevent inflammation, endothelial dysfunction, and platelet activation.

In animal studies, HBA7 was most effective when administered simultaneously with CTH. In this condition, the HBA7 and histone proteins are in the same solution, maximizing their interaction. Nevertheless, there are several insights from this protocol. First, it represents the best-case scenario for HBA7 to neutralize the effect of extracellular histones. If HBA7 did not bind to histones efficiently, the unbound histones would have pathologic effects. By administering them together, our data show that HBA7 is very effective at binding histones, with the capacity to prevent histone-mediated toxicity. Second, these data demonstrate that the histone HBA7 complex does not cause cellular damage.

When HBA7 was delivered 30 min before or after CTH, it protected from disruption of the alveolar barrier but did not prevent WBCs or IL-6 in BALF. This finding suggests that the threshold concentration of histones for barrier disruption is higher than for causing inflammation. In addition, histones have an immediate toxic effect on cells and tissues. Our protocol of delivering HBA7 30 min after CTH allows sufficient time to activate cellular processes prior to potential neutralization by the aptamer. However, this condition does not reflect disease states in which histone proteins are continually released into the extracellular environment. Under pathologic conditions, the administration of HBA7 after the initial pulmonary insult has the potential to neutralize histones and minimize their toxicity. It is notable that after allowing 30 min for CTH to damage the lungs, the administration of HBA7 reduces albumin in the BALF. This observation may, in part, reflect the feedforward effect of histones to cause the additional release of histones.

Another significant limitation of the protocol to deliver HBA7 before or after administration of CTH by oropharyngeal aspiration is the likelihood of unequal distribution of the aptamer and histone proteins. It is likely that alveoli were exposed to CTH but not HBA7. In future studies, and applicable to clinical conditions, the delivery of HBA7 by a nebulizer is expected to provide more uniform distribution throughout the lung.

Smoke inhalation injury is the leading cause of mortality from structure fires and many military combat fields.[40] This study is the first to demonstrate elevated histone levels in BALF from animals subjected to smoke inhalation lung injury. In contrast to the direct delivery of CTH to the lungs, induction of ALI by smoke PM was alleviated by HBA7 regardless of whether the aptamer was delivered before or after the PM. The smoke PM model better reflects clinical scenarios in which there is a sustained production of extracellular histones as opposed to the single bolus of CTH.

Pulmonary delivery of drugs has potential benefits such as increasing local drug concentration and avoiding first-pass metabolism in the liver and kidney. A recent study compared the pulmonary distribution pattern of microspheres in mice when delivered by different pulmonary routes and found that the distribution of microspheres was similar when delivered by oropharyngeal aspiration compared with aerosolization.[39] However, oropharyngeal aspiration had more deposition of the microspheres in the oral cavity. One of the limitations of this study is that we only tested the aptamer efficacy with oropharyngeal aspiration. However, aerosolization is a clinically relevant pulmonary route for drug delivery. Therefore, we expect the delivery to be more efficient with aerosolization.

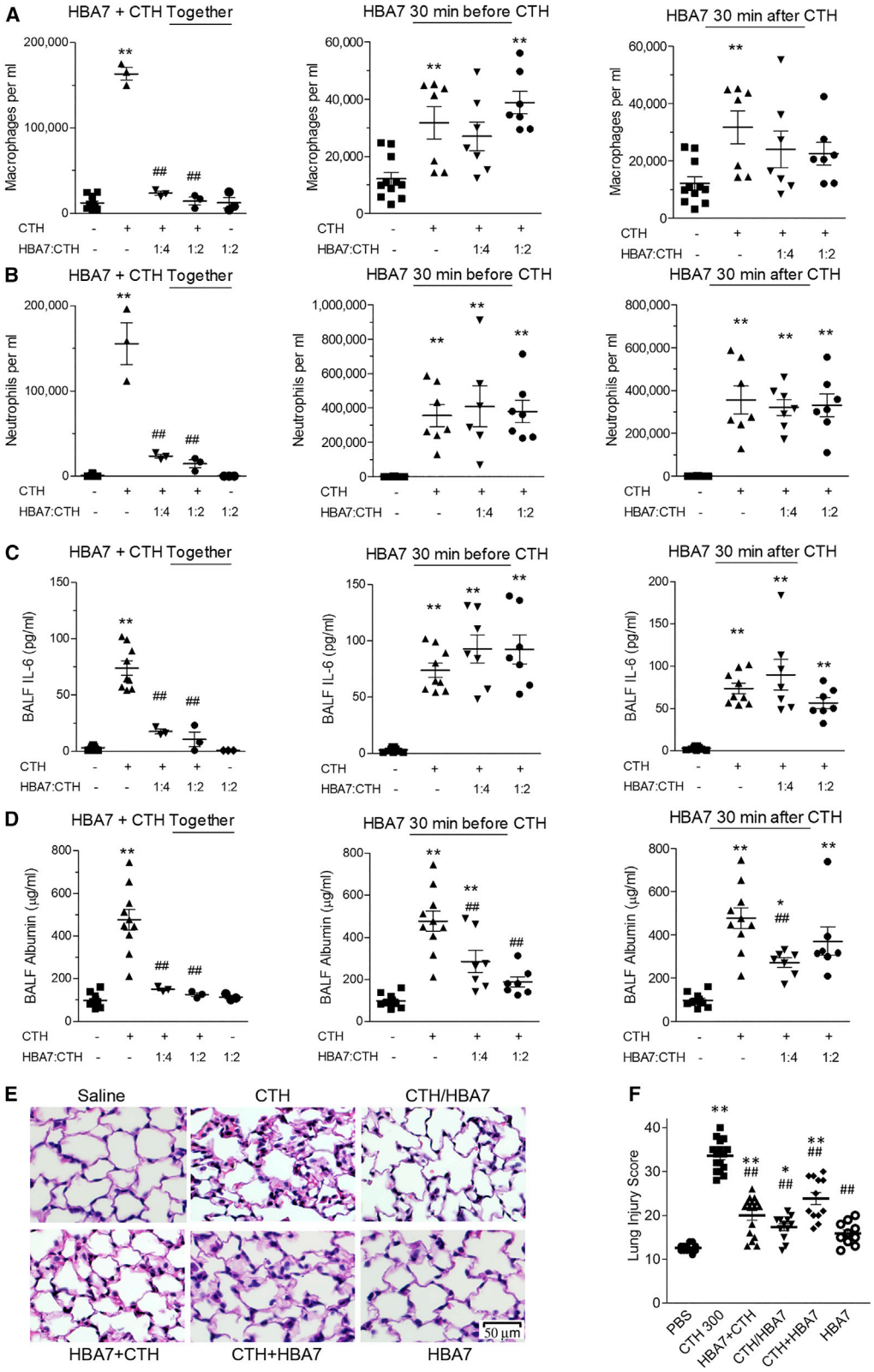

(legend on next page)

We show that HBA7 remained in the lung following inhalation for at least 24 h and did not induce detectable toxicity. This is an advantage over intravenous delivery, in which aptamers have a much shorter half-life due to rapid hepatic and renal clearance. To further protect from degradation, the 2′-hydroxyl (OH) group in the ribose ring of HBA7 is substituted by 2′-Fluoro, affording a high degree of stability.[42] We previously demonstrated HBA7 to have a half-life of >150 h in 50% human serum.[16]

We did not use a scrambled aptamer as a control in our studies. Instead, the control for HBA7 was the vehicle containing no aptamer. A scrambled aptamer retains its negative charge and will bind positively charged histones, albeit at a lower affinity than HBA7. Conditions introduced during systematic evolution of ligands by exponential enrichment (SELEX) allowed for the identification of an RNA aptamer with a high affinity toward H3 and H4 while having a low affinity to other serum proteins. Based on prior testing, we have identified HBA7 as a lead candidate for neutralizing extracellular histones. Furthermore, a scrambled aptamer has the potential to elicit off-target effects (e.g., TLR activation).

Various treatments targeting extracellular histones, including antibodies,[15,43] activated protein C (APC),[15] recombinant thrombomodulin,[44] heparin,[45,46] and C1 esterase inhibitor,[9] have demonstrated efficacy in animal models of ALI. However, each of these approaches has limitations. For example, APC and heparin have an increased risk of bleeding due to nonspecific effects, and APC has failed in clinical trials.[47] In addition, recombinant proteins and antibodies risk allergic reactions and autoimmunity and require special handling and storage at low temperatures. Compared with other biologics, histone-binding RNA aptamers have several advantages: (1) they are chemically synthesized and easy to produce; (2) they have specific targets, which minimizes the potential for off-target effects; (3) they are chemically modified to improve resistance to nuclease-mediated degradation and reduce immunogenicity; (4) they are stable at ambient temperature and available for rapid and easy delivery in field situations; and (5) they are cross-species reactive, facilitating translation to clinical trials.

In summary, inhalation of a histone-binding RNA aptamer protects against histone-mediated lung toxicity and may have therapeutic potential in multiple causes of ALI.

MATERIALS AND METHODS

Reagents

High-glucose Dulbecco's modified Eagle medium (DMEM) (11965), phenol red-free DMEM (31053), L-glutamine (25030-081), penicillin/streptomycin (15140-122), and Opti-MEM (11058-021) (Gibco, Grand Island, NY, USA); EGM-2-MV BulletKit (CC-3202) (Lonza, Walkersville, MD, USA); fetal bovine serum (FBS; F2442), CTH (H9250), and thiazolyl blue tetrazolium bromide (MTT, M2128) (Sigma, St. Louis, MO, USA); dimethyl sulfoxide (DMSO; 0231) (VWR, Solon, OH, USA); Muse Annexin V and dead cell kit (MCH100105) (Millipore, Billerica, MA, USA); RNeasy Mini Kit (74,106) (Qiagen, Valencia, CA, USA); SuperScript III first-strand synthesis SuperMix (18080-400) 4% paraformaldehyde (PFA; J19943-K2), and SuperSignal West Femto Maximum Sensitivity Substrate (34,095) (Thermo Fisher Scientific, Waltham, MA, USA); Power SYBR Green Master mix (4,367,659) (Applied Biosystems, Foster City, CA, USA); PE mouse anti-human CD62P (561,921) (BD Bioscience, San Jose, CA, USA); histone H3 (D1H2) XP Rabbit mAb (4499) (Cell Signaling, Beverly, MA, USA); goat anti-rabbit immunoglobulin G (IgG) HRP (sc-2004) (Santa Cruz Biotechnology, Santa Cruz, CA, USA); mouse tumor necrosis factor α (TNF-α; DY410), IL-1β/IL-1F2 (DY401), IL-6 (DY406), human IL-6 (DY206), human IL-1β/IL-1F2 (DY201), human ICAM1/CD54 (DY720), and human vWF-A2 (DY2764) Duoset ELISA kits (R&D Systems, Minneapolis, MN, USA); mouse albumin ELISA kit (E-90AL) (Immunology Consultants Laboratory, Portland, OR, USA); and RNA aptamers HBA7 and Alexa 647-HBA7 were chemically synthesized by TriLink Biotechnologies (San Diego, CA, USA) or Integrated DNA Technologies (Coralville, IA, USA) with 2′ fluoro pyrimidines. Aptamers were reconstituted in sterile ultrapure H_2O and diluted to a working solution with culture media or PBS.

Cell culture and treatments

Immortal human endothelial cell line EA.hy926 and human lung epithelial cell line A549 were obtained from ATCC (Manassas, VA, USA) and cultured in DMEM supplemented with 10% FBS and 1× penicillin/streptomycin. HPMVECs from Lonza were cultured in EGM-2-MV BulletKit medium (Lonza). All cells were cultured in a humidified atmosphere containing 5% CO_2 at 37°C. Prior to all experiments, cells were seeded in 96-, 12-, or 6-well plates in complete culture medium for 1–2 days and then washed and transferred to serum-free and no-phenol-red DMEM with 1× L-glutamine (EA.hy926 and A549 cells) or Opit-MEM (HPMVECs) for CTH (50 or 75 μg/mL) and/or HBA7 treatment. HBA7 was added to cells 30 to 60 min after CTH exposure.

In vitro cytotoxicity assay

Cell metabolic activity was measured by MTT assay. Briefly, cells were seeded in 96-well plates. After 24 (EA.hy926 or A549 cells) or 4 h (HPMVECs) of histone challenge, cell media was replaced with 0.5 mg/mL MTT in serum-free and phenol-free DMEM (EA.hy926 or A549 cells) or Opti-MEM (HPMVECs). After 4 h of MTT incubation, media were removed, and cells were dissolved in 100 μL DMSO for 5 min at 37°C, and then the absorbance was read at 560 nm with

Figure 5. Inhalation of HBA7 protects from histone-mediated acute lung injury in mice

C57BL/6 mice were subjected to oropharyngeal aspiration of CTHs (300 μg). HBA7 was delivered at the indicated times. Tissues and bronchoalveolar fluid (BALF) were collected 8 h after the CTH challenge for measurement of macrophage and neutrophil numbers (A and B) and IL-6 and albumin concentrations (C and D). The ratio refers to the molar ratio of HBA7 to CTH. In (A)–(D), n = 4–11. Representative microscopic images from H&E-stained lung sections, scale bar is 50 μm (E). Histopathology was scored in a blinded fashion and summarized (F), n = 10–16. HBA7 (86 μg) was delivered by aspiration at 30 min before (HBA7+CTH), at the same time as (CTH/HBA7), or 30 min after (CTH+HBA7) histones. Data are mean ± SEM. *$p < 0.05$, **$p < 0.01$ vs. vehicle control; #$p < 0.05$, ##$p < 0.01$ vs. CTH.

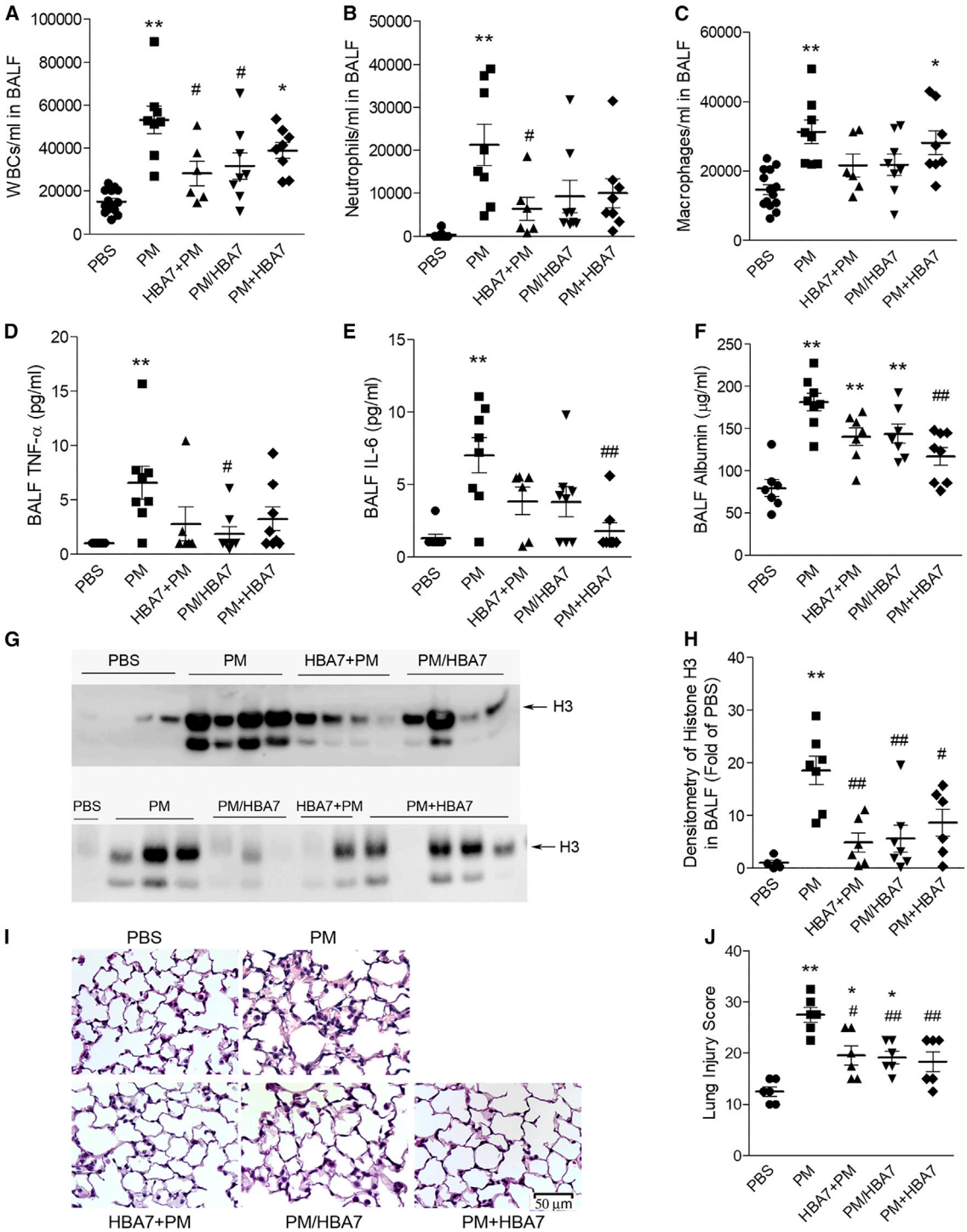

Figure 6. Inhalation of HBA7 reduces smoke particulate matter-mediated lung inflammation and histone accumulation in mice

C57BL/6N mice inhaled smoke particulate matter (PM, 150 μg) via oropharyngeal aspiration. White blood cell counts (A) and differentials (B and C), cytokines TNF-α (D) and IL-6 (E), albumin (F), and histone H3 (G and H) were measured in BALF 24 h after wood smoke challenge. In (G), each lane of the western blot represents BALF from a different mouse. n = 5–10 for (A)–(H). Representative microscopic images from H&E-stained lung sections are shown (scale bar is 50 μm) (I), and histopathology was scored in a blinded fashion (J), n = 6. HBA7 (86 μg) was delivered 30 min before (HBA7+PM), at the same time as (PM/HBA7), or 30 min after (PM+HBA7) smoke matter exposure. Data are mean ± SEM. *$p < 0.05$, **$p < 0.01$ vs. PBS; #$p < 0.05$, ##$p < 0.01$ vs. CTH.

750 nm as the reference wavelength using a plate reader (Turner Biosystems, Sunnyvale, CA, USA). Each treatment was conducted in 3–6 replicates.

For early apoptosis assessment, cells were seeded in 12- or 6-well plates and treated with CTH and/or HBA7. Cells were trypsinized at the indicated times, and early apoptosis was measured using the Muse Annexin V and dead cell kit and analyzed by a Muse Cell Analyzer (Millipore) according to the manufacturer's instruction.

Cytokine induction

Cells were seeded in 6-well plates and treated with CTH and/or HBA7. At 4 h of CTH exposure, cell supernatants were collected for ICAM and vWF ELISAs, and cells were lysed for RNA extraction using a RNeasy Mini Kit (Qiagen). The RNA was reverse transcribed into first-strand cDNA using SuperScript III first-strand synthesis SuperMix (ThermoFisher Scientific). The cDNAs were used in real-time PCR to quantify the mRNA expression levels of proinflammatory cytokine genes IL-1β and IL-6. Each reaction was performed in triplicate in a 10 μL volume with Power SYBR Green (Applied Biosystems) and programmed in CFX384 Touch Real-Time PCR Detection System (Bio-Rad, Hercules, CA, USA) as follows: 95°C for 10 min, 40 cycles of 95°C for 15 s, and 60°C for 50 s, followed by a melting curve 95°C for 15 s, 60°C for 1 min, and 95°C for 1 s. Relative gene expression data were calculated using GAPDH as a reference. The mouse-specific primers used were IL-1β (forward: 5'-GCT TAT TAC AGT GGC AAT GAG-3'; reverse: 5'-GTA GTG GTG GTC GGA GAT TC-3'), IL-6 (forward: 5'-AGA CAG CCA CTC ACC TCT TCA G-3'; reverse: 5'-TTC TGC CAG TGC CTC TTT GCT G-3'), and GAPDH (forward: 5'-TGC CAA ATA TGA TGA CAT CAA GA-3'; reverse: 5'-GGA GTG GGT GTC GCT GTT-3').

Quantification of ICAM and vWF production

Cell supernatants were collected and centrifuged at 10,000 × *g* for 1 min to exclude particulates. ICAM and vWF were measured in the supernatant by ELISA using commercially available kits (R&D Systems) according to the manufacturer's instructions.

Human platelet isolation and activation

Human blood was collected under a protocol (PRO 00014281) approved by the Durham Veterans Affairs Medical Center Institutional Review Board, and written consent was obtained. Venous blood (10 mL) was collected from healthy donors. Platelets were isolated by density gradient centrifugation and purified by gel filtration as described previously.[48] Platelet activation was determined by the expression levels of platelet surface marker P-selectin. Briefly, 200 μL f purified platelets were incubated at 37°C with thrombin (10 nM) for 5 min or CTH (50 μg/mL) for 15 min in the presence or absence of HBA7, and reactions were stopped by the addition of 200 μL 2% PFA. After 30 min of fixation at room temperature, 800 μL HEPES-buffered saline (HBS; pH7.4) containing 1 mg/mL BSA and 3 mM $CaCl_2$ was added to each sample for 1 h. Platelets were centrifuged and resuspended in 50 μL HBS containing a P-selectin antibody (PE mouse anti-human CD62P, 1:50). After 30 min of incubation at room temperature, 500 μL HBS was added to each sample, and P-selectin expression was analyzed using a FACSCAN flow cytometer (Becton Dickinson, Franklin Lakes, NJ, USA).[48,49]

Animal experiments

The research using animals adhered to the laws of the United States regulations of the Department of Agriculture and Department of Defense. Experiments were designed to minimize animal discomfort and numbers, conformed to international guidelines on the use of animals, and were approved by the Duke University Institutional Animal Care and Use Committee (protocol A185-16-08) and by the US Army Medical Research Materiel Command Animal Care and Use Review Office (protocol PR150627). C57BL/6N male mice at the age of 10 weeks (Charles River, Morrisville, NC, USA) were housed on a 12 h light/dark cycle in standard acrylic cages with *ad libitum* access to water and food (Lab Diet 5001, PMI Nutrition International, St. Louis, MO, USA).

The animal studies were conducted by the Duke Rodent Inhalation and Physiology Core. C57BL/6N male mice were randomly assigned to treatment groups at 10 weeks of age (Charles River, Morrisville, NC, USA). Oropharyngeal delivery to mice was performed by the aspiration of 50 μL solutions under isoflurane anesthesia. For histone-induced lung injury, mice were challenged via oropharyngeal aspiration with 300 μg CTH or PBS and euthanized 8 h later. For the wood smoke lung injury model, 150 μg eucalyptus flaming smoke PM (provided by Ian Gilmour at the EPA, Cary, NC, USA)[41] or PBS was delivered by oropharyngeal aspiration, and mice were sacrificed 24 h after exposure. HBA7 or saline was delivered via oropharyngeal aspiration at indicated times. HBA7, or vehicle, was delivered to mice via oropharyngeal aspiration.

Anesthesia via intraperitoneal injection of ketamine (100 mg/kg) and xylazine (10 mg/kg) was used for tissue harvest. BALF was collected[50] to assess total cell counts and differentials, albumin, and cytokine levels. Organs were sectioned to evaluate the distribution of Alexa 647-HBA7 or stained with hematoxylin and eosin for evaluation of histopathological injury.[51] Group assignment was masked from the investigators carrying out tissue harvest, BALF analysis, and lung histopathological assessment.

Aptamer distribution and retention

The fluorescent-tagged aptamer Alexa 647-HBA7 (1.7 nmol, 30 μg) was delivered to mice via oropharyngeal aspiration. At 4 and 24 h after aptamer administration, mice were anesthetized with ketamine/xylazine injection, blood was drawn for plasma from descending aorta, the lung was infused through tracheal with PBS by 20 cm H_2O gravity, and BALF was collected by passive drainage as described previously.[50] After perfusing the lung with PBS, the left lobe was dissected, and half was frozen in liquid nitrogen, while the other half was placed in 4% PFA. The right lung was inflated and fixed with 4% PFA. Heart, liver, spleen, kidney, and brain were removed and divided, with half being flash-frozen in liquid nitrogen and half fixed in 4% PFA. After 5 h of fixation, tissues were transferred into

30% sucrose in PBS for 24 h at 4°C. Frozen 10 μm sections were sliced with a cryostat and mounted onto charged slides. The distribution of Alexa 647-HBA7 was observed under an IX73 fluorescent microscope (Olympus, Waltham, MA, USA), and images were acquired. HBA7 retention in the BALF was estimated via fluorescence intensity measurement at 630 nm. HBA7 retention in the lung was determined by the recovery of HBA7 from lung tissue and BALF via RT-PCR as previously described.[52]

BALF analysis

BALF was collected and centrifuged at 3,000 RPM at 4°C for 10 min. The supernatant, cell-free BALF was transferred and stored at −80°C until further analysis. The cell pellet was resuspended in PBS, and then total WBCs were counted with a cellometer, and cells were stained with Diff Quick for differential analysis. A mouse albumin ELISA kit (Immunology Consultants Laboratory) measured albumin levels. BALF cytokines TNF-α, IL-1β, and IL-6 were measured by ELISA using commercially available kits (R&D Systems) per the manufacturer's protocol.

Lung histology

The right lung was inflated through the trachea with 4% PFA, transferred to 4% PFA at 4°C for 24 h, and then paraffin embedded. Tissue sections (5 μm) were stained with hematoxylin and eosin. Images of 5 random fields were taken from each lobe of the right lung (20 random fields/animal) under an IX73 microscope (Olympus, Waltham, MA, USA). Histological sections from each lobe were scored for severity of injury (none, mild, moderate, severe) based on criteria previously described.[51] Individuals scoring the sections were blinded to the treatments.

Measurement of histones in BALF

BALF histone levels were measured by western blot analysis. Cell-free BALF was mixed with 4× LDS sample buffer containing 200 mM DTT and heated at 95°C for 5 min. An equivalent amount of each sample was loaded and resolved on a 4%–12% Bis-Tris PAGE gel at 200 V for 35 min and transferred to nitrocellulose membranes at 30 V for 40 min. Blots were blocked in 5% BSA-TBS for 1 h, incubated with anti-histone H3 antibody (Ab; 1:2,000) for 1 h in 2% BSA-TBS-0.2% Tween 20, and then incubated with goat anti-rabbit HRP (1:10,000) for 1 h. The signal was detected using SuperSignal West Femto Maximum Sensitivity Substrate and imaged with an imaging system (LI-COR Biosciences, Lincoln, NE, USA).

Statistical analysis

Results are expressed as the mean ± standard error, compiled from n independent experiments. Statistical significance was analyzed by analysis of variance followed by Bonferroni post-test. All calculations were performed using GraphPad Prism v.9.5 (GraphPad Software, San Diego, CA, USA), with $p < 0.05$ considered significant.

DATA AVAILABILITY

The data that support the findings of this study are available upon reasonable request to the corresponding authors.

SUPPLEMENTAL INFORMATION

Supplemental information can be found online at https://doi.org/10.1016/j.omtn.2023.02.021.

ACKNOWLEDGMENTS

The authors thank Jaime Daly and Barbara Theriot at the Duke Rodent Inhalation and Physiology Core Resource Facility (Duke University, Durham, NC, USA) for their technical assistance with the mouse lung injury models. In addition, we thank Ian Gilmour at Public Health and Integrated Toxicology Division, Center for Public Health and Environmental Assessment, US Environmental Protection Agency (Research Triangle Park, NC, USA), for kindly providing eucalyptus flaming particulate smoke matter. This work was supported by the Office of the Assistant Secretary of Defense for Health Affairs and the Defense Health Agency J9, Research and Development Directorate, through the Congressionally Directed Medical Research Programs (CDMRP) under award no. (W81XWH-16-1-0179 to F.J.M. and W81XWH-16-1-0180 to P.H.G.), and the Department of Veterans Affairs, Veterans Health Administration, Office of Research and Development, Biomedical Laboratory Research and Development (BX005450). The contents of this manuscript are new and solely the authors' responsibility and do not necessarily represent the official views of the granting agencies.

AUTHOR CONTRIBUTIONS

B.L., P.H.G., and F.J.M. designed research studies. B.L., C.W., K.S., R.M.T., A.M.F., and M.R.H. conducted experiments. M.G., B.L., and F.J.M. performed lung histopathological scoring. B.L. and F.J.M. analyzed data and wrote the manuscript.

DECLARATION OF INTERESTS

The authors declare no competing interests.

REFERENCES

1. Thompson, B.T., Chambers, R.C., and Liu, K.D. (2017). Acute respiratory distress syndrome. N. Engl. J. Med. *377*, 562–572.
2. Mokra, D., and Kosutova, P. (2015). Biomarkers in acute lung injury. Respir. Physiol. Neurobiol. *209*, 52–58.
3. Rubenfeld, G.D., Caldwell, E., Peabody, E., Weaver, J., Martin, D.P., Neff, M., Stern, E.J., and Hudson, L.D. (2005). Incidence and outcomes of acute lung injury. N. Engl. J. Med. *353*, 1685–1693.
4. Abrams, S.T., Zhang, N., Manson, J., Liu, T., Dart, C., Baluwa, F., Wang, S.S., Brohi, K., Kipar, A., Yu, W., et al. (2013). Circulating histones are mediators of trauma-associated lung injury. Am. J. Respir. Crit. Care Med. *187*, 160–169.
5. Zhang, Y., Wen, Z., Guan, L., Jiang, P., Gu, T., Zhao, J., Lv, X., and Wen, T. (2015). Extracellular histones play an inflammatory role in acid aspiration-induced acute respiratory distress syndrome. Anesthesiology *122*, 127–139.
6. Lefrançais, E., Mallavia, B., Zhuo, H., Calfee, C.S., and Looney, M.R. (2018). Maladaptive role of neutrophil extracellular traps in pathogen-induced lung injury. JCI Insight *3*, e98178.
7. Lv, X., Wen, T., Song, J., Xie, D., Wu, L., Jiang, X., Jiang, P., and Wen, Z. (2017). Extracellular histones are clinically relevant mediators in the pathogenesis of acute respiratory distress syndrome. Respir. Res. *18*, 165.
8. Bosmann, M., Grailer, J.J., Ruemmler, R., Russkamp, N.F., Zetoune, F.S., Sarma, J.V., Standiford, T.J., and Ward, P.A. (2013). Extracellular histones are essential effectors of C5aR- and C5L2-mediated tissue damage and inflammation in acute lung injury. Faseb. J. *27*, 5010–5021.

9. Wygrecka, M., Kosanovic, D., Wujak, L., Reppe, K., Henneke, I., Frey, H., Didiasova, M., Kwapiszewska, G., Marsh, L.M., Baal, N., et al. (2017). Antihistone properties of C1 esterase inhibitor protect against lung injury. Am. J. Respir. Crit. Care Med. *196*, 186–199.

10. Claushuis, T.A.M., van der Donk, L.E.H., Luitse, A.L., van Veen, H.A., van der Wel, N.N., van Vught, L.A., Roelofs, J.J.T.H., de Boer, O.J., Lankelma, J.M., Boon, L., et al. (2018). Role of peptidylarginine deiminase 4 in neutrophil extracellular trap formation and host Defense during Klebsiella pneumoniae-induced pneumonia-derived sepsis. J. Immunol. *201*, 1241–1252.

11. Biterge, B., and Schneider, R. (2014). Histone variants: key players of chromatin. Cell Tissue Res. *356*, 457–466.

12. Karki, P., Birukov, K.G., and Birukova, A.A. (2020). Extracellular histones in lung dysfunction: a new biomarker and therapeutic target? Pulm. Circ. *10*. 2045894020965357.

13. Delgado-Rizo, V., Martínez-Guzmán, M.A., Iñiguez-Gutierrez, L., García-Orozco, A., Alvarado-Navarro, A., and Fafutis-Morris, M. (2017). Neutrophil extracellular traps and its implications in inflammation: an overview. Front. Immunol. *8*, 81.

14. Nair, R.R., Mazza, D., Brambilla, F., Gorzanelli, A., Agresti, A., and Bianchi, M.E. (2018). LPS-challenged macrophages release microvesicles coated with histones. Front. Immunol. *9*, 1463.

15. Xu, J., Zhang, X., Pelayo, R., Monestier, M., Ammollo, C.T., Semeraro, F., Taylor, F.B., Esmon, N.L., Lupu, F., and Esmon, C.T. (2009). Extracellular histones are major mediators of death in sepsis. Nat. Med. *15*, 1318–1321.

16. Urak, K.T., Blanco, G.N., Shubham, S., Lin, L.H., Dassie, J.P., Thiel, W.H., Chen, Y., Sonkar, V.K., Lei, B., Murthy, S., et al. (2019). RNA inhibitors of nuclear proteins responsible for multiple organ dysfunction syndrome. Nat. Commun. *10*, 116.

17. Xu, J., Zhang, X., Monestier, M., Esmon, N.L., and Esmon, C.T. (2011). Extracellular histones are mediators of death through TLR2 and TLR4 in mouse fatal liver injury. J. Immunol. *187*, 2626–2631.

18. Huang, H., Evankovich, J., Yan, W., Nace, G., Zhang, L., Ross, M., Liao, X., Billiar, T., Xu, J., Esmon, C.T., and Tsung, A. (2011). Endogenous histones function as alarmins in sterile inflammatory liver injury through Toll-like receptor 9 in mice. Hepatology *54*, 999–1008.

19. Allam, R., Scherbaum, C.R., Darisipudi, M.N., Mulay, S.R., Hägele, H., Lichtnekert, J., Hagemann, J.H., Rupanagudi, K.V., Ryu, M., Schwarzenberger, C., et al. (2012). Histones from dying renal cells aggravate kidney injury via TLR2 and TLR4. J. Am. Soc. Nephrol. *23*, 1375–1388.

20. Zhang, Y., Guan, L., Yu, J., Zhao, Z., Mao, L., Li, S., and Zhao, J. (2016). Pulmonary endothelial activation caused by extracellular histones contributes to neutrophil activation in acute respiratory distress syndrome. Respir. Res. *17*, 155.

21. Ammollo, C.T., Semeraro, F., Xu, J., Esmon, N.L., and Esmon, C.T. (2011). Extracellular histones increase plasma thrombin generation by impairing thrombomodulin-dependent protein C activation. J. Thromb. Haemostasis *9*, 1795–1803.

22. Michels, A., Albánez, S., Mewburn, J., Nesbitt, K., Gould, T.J., Liaw, P.C., James, P.D., Swystun, L.L., and Lillicrap, D. (2016). Histones link inflammation and thrombosis through the induction of Weibel-Palade body exocytosis. J. Thromb. Haemostasis *14*, 2274–2286.

23. Gould, T.J., Lysov, Z., Swystun, L.L., Dwivedi, D.J., Zarychanski, R., Fox-Robichaud, A.E., and Liaw, P.C.; Canadian Critical Care Translational Biology Group (2016). Extracellular histones increase tissue factor activity and enhance thrombin generation by human blood monocytes. Shock *46*, 655–662.

24. Perdomo, J., Leung, H.H.L., Ahmadi, Z., Yan, F., Chong, J.J.H., Passam, F.H., and Chong, B.H. (2019). Neutrophil activation and NETosis are the major drivers of thrombosis in heparin-induced thrombocytopenia. Nat. Commun. *10*, 1322.

25. Abrams, S.T., Su, D., Sahraoui, Y., Lin, Z., Cheng, Z., Nesbitt, K., Alhamdi, Y., Harrasser, M., Du, M., Foley, J.H., et al. (2021). Assembly of alternative prothrombinase by extracellular histones initiates and disseminates intravascular coagulation. Blood *137*, 103–114.

26. Tuerk, C., and Gold, L. (1990). Systematic evolution of ligands by exponential enrichment: RNA ligands to bacteriophage T4 DNA polymerase. Science *249*, 505–510.

27. Ellington, A.D., and Szostak, J.W. (1990). In vitro selection of RNA molecules that bind specific ligands. Nature *346*, 818–822.

28. Chan, M.Y., Rusconi, C.P., Alexander, J.H., Tonkens, R.M., Harrington, R.A., and Becker, R.C. (2008). A randomized, repeat-dose, pharmacodynamic and safety study of an antidote-controlled factor IXa inhibitor. J. Thromb. Haemostasis *6*, 789–796.

29. Sundaram, P., Kurniawan, H., Byrne, M.E., and Wower, J. (2013). Therapeutic RNA aptamers in clinical trials. Eur. J. Pharmaceut. Sci. *48*, 259–271.

30. Lei, B., Snow, K., Fang, J., Tighe, R.M., Giangrande, P.H., and Miller, F.J. (2019). Inhalation of an RNA aptamer targeting extracellular histones protects from acute lung injury. Mol. Ther. *27*, 334.

31. Ochoa, C.D., Wu, S., and Stevens, T. (2010). New developments in lung endothelial heterogeneity: von Willebrand factor, P-selectin, and the Weibel-Palade body. Semin. Thromb. Hemost. *36*, 301–308.

32. Pulavendran, S., Rudd, J.M., Maram, P., Thomas, P.G., Akhilesh, R., Malayer, J.R., Chow, V.T.K., and Teluguakula, N. (2019). Combination therapy targeting platelet activation and virus replication protects mice against lethal influenza pneumonia. Am. J. Respir. Cell Mol. Biol. *61*, 689–701.

33. Liao, J.K. (2013). Linking endothelial dysfunction with endothelial cell activation. J. Clin. Invest. *123*, 540–541.

34. Lowenstein, C.J., Morrell, C.N., and Yamakuchi, M. (2005). Regulation of Weibel-Palade body exocytosis. Trends Cardiovasc. Med. *15*, 302–308.

35. Gragnano, F., Sperlongano, S., Golia, E., Natale, F., Bianchi, R., Crisci, M., Fimiani, F., Pariggiano, I., Diana, V., Carbone, A., et al. (2017). The role of von Willebrand factor in vascular inflammation: from pathogenesis to targeted therapy. Mediat. Inflamm. *2017*, 5620314.

36. Hsu-Lin, S., Berman, C.L., Furie, B.C., August, D., and Furie, B. (1984). A platelet membrane protein expressed during platelet activation and secretion. Studies using a monoclonal antibody specific for thrombin-activated platelets. J. Biol. Chem. *259*, 9121–9126.

37. Merten, M., and Thiagarajan, P. (2000). P-selectin expression on platelets determines size and stability of platelet aggregates. Circulation *102*, 1931–1936.

38. Carestia, A., Rivadeneyra, L., Romaniuk, M.A., Fondevila, C., Negrotto, S., and Schattner, M. (2013). Functional responses and molecular mechanisms involved in histone-mediated platelet activation. Thromb. Haemostasis *110*, 1035–1045.

39. Kunda, N.K., Price, D.N., and Muttil, P. (2018). Respiratory tract deposition and distribution pattern of microparticles in mice using different pulmonary delivery techniques. Vaccines *6*, 41.

40. Demling, R.H. (2008). Smoke inhalation lung injury: an update. Eplasty *8*, e27.

41. Hargrove, M.M., Kim, Y.H., King, C., Wood, C.E., Gilmour, M.I., Dye, J.A., and Gavett, S.H. (2019). Smoldering and flaming biomass wood smoke inhibit respiratory responses in mice. Inhal. Toxicol. *31*, 236–247.

42. Kratschmer, C., and Levy, M. (2017). Effect of chemical modifications on aptamer stability in serum. Nucleic Acid Therapeut. *27*, 335–344.

43. Ashar, H.K., Mueller, N.C., Rudd, J.M., Snider, T.A., Achanta, M., Prasanthi, M., Pulavendran, S., Thomas, P.G., Ramachandran, A., Malayer, J.R., et al. (2018). The role of extracellular histones in influenza virus pathogenesis. Am. J. Pathol. *188*, 135–148.

44. Nakahara, M., Ito, T., Kawahara, K.i., Yamamoto, M., Nagasato, T., Shrestha, B., Yamada, S., Miyauchi, T., Higuchi, K., Takenaka, T., et al. (2013). Recombinant thrombomodulin protects mice against histone-induced lethal thromboembolism. PLoS One *8*, e75961.

45. Wildhagen, K.C.A.A., García de Frutos, P., Reutelingsperger, C.P., Schrijver, R., Aresté, C., Ortega-Gómez, A., Deckers, N.M., Hemker, H.C., Soehnlein, O., and Nicolaes, G.A.F. (2014). Nonanticoagulant heparin prevents histone-mediated cytotoxicity in vitro and improves survival in sepsis. Blood *123*, 1098–1101.

46. Zhang, Y., Zhao, Z., Guan, L., Mao, L., Li, S., Guan, X., Chen, M., Guo, L., Ding, L., Cong, C., et al. (2014). N-acetyl-heparin attenuates acute lung injury caused by acid aspiration mainly by antagonizing histones in mice. PLoS One *9*, e97074.

47. Martí-Carvajal, A.J., Solà, I., Lathyris, D., and Cardona, A.F. (2012). Human Recombinant Activated Protein C for Severe Sepsis (Cochrane Database Syst Rev), p. Cd004388.

48. Hoffman, M., Monroe, D.M., and Roberts, H.R. (1992). A rapid method to isolate platelets from human blood by density gradient centrifugation. Am. J. Clin. Pathol. *98*, 531–533.

49. Fager, A.M., Machlus, K.R., Ezban, M., and Hoffman, M. (2018). Human platelets express endothelial protein C receptor, which can be utilized to enhance localization of factor VIIa activity. J. Thromb. Haemostasis *16*, 1817–1829.

50. Tighe, R.M., Birukova, A., Yaeger, M.J., Reece, S.W., and Gowdy, K.M. (2018). Euthanasia- and lavage-mediated effects on bronchoalveolar measures of lung injury and inflammation. Am. J. Respir. Cell Mol. Biol. *59*, 257–266.

51. Matute-Bello, G., Downey, G., Moore, B.B., Groshong, S.D., Matthay, M.A., Slutsky, A.S., and Kuebler, W.M.; Acute Lung Injury in Animals Study Group (2011). An official American Thoracic Society workshop report: features and measurements of experimental acute lung injury in animals. Am. J. Respir. Cell Mol. Biol. *44*, 725–738.

52. Thiel, W.H., Thiel, K.W., Flenker, K.S., Bair, T., Dupuy, A.J., McNamara, J.O., 2nd, Miller, F.J., and Giangrande, P.H. (2015). Cell-internalization SELEX: method for identifying cell-internalizing RNA aptamers for delivering siRNAs to target cells. Methods Mol. Biol. *1218*, 187–199.